Journal of Materials Chemistry B

PAPER

View Article Online
View Journal | View Issue

Cite this: J. Mater. Chem. B, 2015, 3, 5569

A fast degradable citrate-based bone scaffold promotes spinal fusion

Jiajun Tang,†[ab] Jinshan Guo,†[c] Zhen Li,[ab] Cheng Yang,[ab] Denghui Xie,[ab] Jian Chen,[ab] Shengfa Li,[ab] Shaolin Li,[d] Gloria B. Kim,[c] Xiaochun Bai,*[ab] Zhongmin Zhang*[a] and Jian Yang*[c]

Received 2nd April 2015,
Accepted 3rd June 2015

DOI: 10.1039/c5tb00607d

www.rsc.org/MaterialsB

It is well known that high rates of fusion failure and pseudoarthrosis development (5–35%) are concomitant in spinal fusion surgery, which was ascribed to the shortage of suitable materials for bone regeneration. Citrate was recently recognized to play an indispensable role in enhancing osteoconductivity and osteoinductivity, and promoting bone formation. To address the material challenges in spinal fusion surgery, we have synthesized mechanically robust and fast degrading citrate-based polymers by incorporating *N*-methyldiethanolamine (MDEA) into clickable poly(1,8-octanediol citrates) (POC-click), referred to as POC-M-click. The obtained POC-M-click were fabricated into POC-M-click–HA matchstick scaffolds by forming composites with hydroxyapatite (HA) for interbody spinal fusion in a rabbit model. Spinal fusion was analyzed by radiography, manual palpation, biomechanical testing, and histological evaluation. At 4 and 8 weeks post surgery, POC-M-click–HA scaffolds showed optimal degradation rates that facilitated faster new bone formation and higher spinal fusion rates (11.2 ± 3.7, 80 ± 4.5 at week 4 and 8, respectively) than the poly(L-lactic acid)–HA (PLLA–HA) control group (9.3 ± 2.4 and 71.1 ± 4.4) ($p < 0.05$). The POC-M-click–HA scaffold-fused vertebrates possessed a maximum load and stiffness of 880.8 ± 14.5 N and 843.2 ± 22.4 N mm^{-1}, respectively, which were also much higher than those of the PLLA–HA group (maximum: 712.0 ± 37.5 N, stiffness: 622.5 ± 28.4 N mm^{-1}, $p < 0.05$). Overall, the results suggest that POC-M-click–HA scaffolds could potentially serve as promising bone grafts for spinal fusion applications.

1. Introduction

Bone transplantation is the second most common tissue transplant in the world following blood transfusion with over 2.2 million procedures performed annually worldwide.[1,2] 50% of bone transplantation procedures are spine fusion, which has become a routine procedure in the field of spine surgery for the treatment of cervical vertebra instability, lumbar degeneration, intervertebral disc injury, and spinal deformity diseases. Normally, spinal fusion surgery is effective in achieving vertebral stability and nerve decompression.[3] However, the rates of fusion failure and pseudarthrosis development are reported to be as high as 5–35%. The choice of material as an intervertebral filler is extremely critical in spinal fusion surgery in addition to the patient condition and the choice of bone transplantation mode.[4]

The ideal bone substitute should be osteoconductive, osteoinductive, degradable and resorbable, non-immunogenic, risk-free from disease transmission, easy-to-use, mechanically robust, and cost-effective. Up to now, autologous bones remain the best filling material for intervertebral fusion due to their non-immunogenic properties and high intervertebral fusion rates compared to other materials. However, their use is quite limited due to their associated disadvantages, including additional surgical trauma, increased risk of postoperative complications, and limited quantity of suitable autologous bones.[5] Although the application of allograft and xenograft bones solves the problem of limited supply and avoids additional surgical trauma associated with autologous bone harvesting, it brings concerns such as immune rejection and the risk of spread of bone disease.[6–8] Thus, the development of engineered bone substitutes as fillers for intervertebral fusion is greatly encouraged. Examples of engineered bone substitutes include calcium-based and polymer-based synthetic bone substitutes such as hydroxyapatite (HA), β-tricalcium phosphate (β-TCP), poly(L-lactic acid) (PLLA), poly(glycolic acid) (PGA) and their

[a] Academy of Orthopedics, Guangdong Province, Department of Orthopedic Surgery, The Third Affiliated Hospital of Southern Medical University, Guangzhou, 510630, China. E-mail: 13002006619@163.com
[b] Department of Cell Biology, School of Basic Medical Science, Southern Medical University, Guangzhou 510515, China. E-mail: baixc15@smu.edu.cn
[c] Department of Biomedical Engineering, Materials Research Institute, The Huck Institutes of The Life Sciences, The Pennsylvania State University, University Park, PA 16802, USA. E-mail: jxy30@psu.edu
[d] Medical imaging department, Guangdong Province, The Third Affiliated Hospital of Southern Medical University, Guangzhou, 510630, China
† These authors contribute equally to this work.

copolymers, as well as polymer–HA or TCP composites.[9–11] Unfortunately, the successful application of these materials has been hampered by problems such as inherent brittleness, poor degradability, insufficient biocompatibility, low fusion rates, and unsatisfactory biomechanical properties.[12,13] Therefore, the search for a biodegradable, cost-effective, biocompatible, osteoconductive, and even osteoinductive bone substitute material that can be used to achieve a high spinal fusion rate and optimal bone regeneration has become the focus of extensive research.

Citrate, as an important intermediate in the Kreb's cycle, is highly concentrated in native bone (90% of body's total citrate content is located in the skeletal system) and is closely associated with bone metabolism and formation.[2,14–17] Citrate not only serves as a calcium-solubilizing agent, but also plays an important role in the physical binding and thickness control of bone apatite nanocrystals.[15–17] Our recent exciting findings further showed that exogenous citrates enhance alkaline phosphatase (ALP) and osterix (OSX) gene expression in C2C12 cells, a mouse myoblast cell line that can differentiate into osteoblasts,[18] and promote the mineralization of osteoblastic differentiated human mesenchymal stem cells (hMSCs).[19] A series of citrate-based biodegradable composites have recently been developed for bone regeneration, such as poly(1,8-octanediol citrate)–hydroxyapatite (POC–HA),[20,21] clickable POC–HA (POC-click–HA),[2,22] crosslinked urethane-doped polyesters–HA (CUPE–HA),[2] citrate-based polymer blends–HA (CBPBHA),[18] poly(ethylene glycol) maleate citrate–HA (PEGMC–HA),[23] and injectable citrate-based mussel-inspired tissue bioadhesives HA composites (iCMBA–HA).[19] The above citrate-based biomaterials have demonstrated impressive *in vivo* performance in various animal models for bone regeneration, such as POC-click–HA for long segmental radial bone regeneration in rabbits,[22] CUPE–HA and POC-click–HA for calvarial regeneration in rats,[2] and iCMBA–HA for comminuted radial bone regeneration in rabbits.[19] However, none of the citrate-based biodegradable composites have been optimized and evaluated for spinal fusion applications.

Abundant free carboxyl groups provided by citrate polymers can enhance polymer–HA interactions by calcium chelating. Up to 65 wt% HA can be effectively incorporated in citrate-based polymers (*i.e.* POC) to mimic the composition of native bones in contrast to conventional biodegradable polymers (*i.e.* PLLA), into which only up to 35% of HA can be incorporated before the composites become too brittle. This attribute is a remarkable advantage of citrate-based polymers compared to other degradable polymers, but the mechanical strengths of citrate-based polymer–HA composites still need to be improved to meet the requirements for bone applications. To further improve the mechanical strength of citrate-based polymers without sacrificing the valuable free carboxyl groups on citrate, clickable POC (POC-click) with robustly enhanced mechanical strength was recently developed in our lab[24] by employing click chemistry (azide–alkyne cycloaddition) as an additional cross-linking mechanism.

The composites of POC-click with HA did show significantly improved mechanical strengths and enhanced calvarial regeneration in rats.[2,22] However, click reaction resulted in rigid triazole rings, which delayed the degradation of POC-click as compared with normal POC.[24–26]

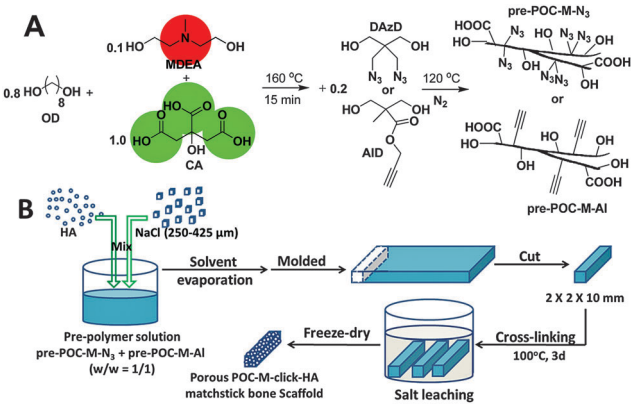

Fig. 1 (A) Synthesis of *N*-methyldiethanolamine (MDEA) modified poly(1,8-octanediol citrate)-click (POC-M-click) pre-polymers: pre-POC-M-N3 and pre-POC-Al. (B) Fabrication process of POC-M-click–HA matchstick bone scaffolds.

In the present paper, a new POC-click polymer with faster degradation, referred to as POC-M-click, was synthesized by introducing *N*-methyldiethanolamine (MDEA), an amine-containing diol (Fig. 1A) in the POC-click backbone. The introduced amine-containing diol can buffer the carboxyl acid groups from citrates, and promote the hydrolysis process. Porous POC-M-click–HA matchstick bone scaffolds were fabricated by forming composites with HA and sodium chloride (as porogen) (Fig. 1B). The performance of the prepared scaffolds as a bone substitute for intervertebral fusion was investigated *in vivo* using a rabbit model (Fig. 2) and compared to the clinical "gold standard", autologous bone graft, and the widely used PLLA–HA.[11,26] The design strategies behind the POC-M-click–HA matchstick spinal fusion scaffolds are as follows: (1) citrate polymer–HA composites can better mimic the citrate and mineral compositions of nature bone compared to the traditional biodegradable non-citrate polymer–HA composites; (2) citrate-based biomaterials can innately promote bone regeneration through the demonstrated citrate effects; (3) MDEA can effectively speed up the degradation of the mechanically strong POC-click polymers to match the rate of bone regeneration; and (4) matchstick scaffolds can be easily manipulated and implanted in the spinal interbody voids to promote spinal fusion.

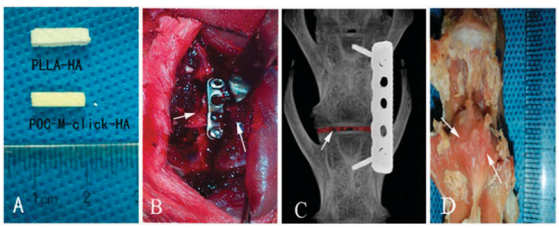

Fig. 2 Implantation of scaffolds in a rabbit interbody fusion model. (A) POC-M-click–HA and PLLA–HA scaffolds prior to implantation. Scaffold size: 2 mm × 2 mm × 10 mm. (B and C) Pictures taken during the operation. (D) Visual observation of successful fusion at 12 weeks. Arrows point to fused vertebrae.

2. Results and discussion

Citrate is an essential constituent in native bone and was found to play an indispensable role in the formation and thickness regulation of the nanocrystalline structure of bone apatite.[15–17] The most recent finding further indicated that citrate incorporation ("citration") in concert with mineralization must be included in the process of bone formation.[27] The existing findings in our group showed that exogenous citrate, in the forms of free citrate salt or citrate-based polymers, can enhance the expression of genes related to bone formation, including alkaline phosphatase (ALP) and osterix (OSX), and promote the mineralization of osteoblastic-committed human mesenchymal stem cells (hMSCs).[18,19] These evolving findings strongly suggest that citrate should be involved in bone substitute design to mimic the structure and function of native bone.

On the other hand, proper mechanical strength, sufficient polymer–ceramic binding, and suitable degradation rates are three key factors for the successful application of biodegradable polymer–bioceramic composites in bone regeneration. Although traditional commercially available biodegradable polymers, such as PLLA, are widely used as bone substitutes, they suffer from ineffective binding to inorganic particles and long degradation times. Complete degradation of PLLA needs more than one year (~52 weeks),[28] which would hinder the bone-healing process by inhibiting new bone and vascular ingrowth.[19]

The existence of abundant free carboxyl groups and the application of click chemistry in POC-click polymers provided them with sufficient binding to bioceramic particles and enhanced mechanical properties.[24] However, the rigid triazole rings in crosslinked POC-click delayed the degradation. To preserve higher mechanical strength and generate faster degradation rate, an amine-containing diol, *N*-methyldiethanol-amine (MDEA), was introduced into POC-click pre-polymers to obtain pre-POC-M-N_3 and pre-POC-M-Al (Fig. 1A). By cross-linking the equal-weight mixture of pre-POC-M-N_3 and pre-POC-M-Al, crosslinked POC-M-click was obtained. As shown in Fig. 3A, the degradation rate of POC-M-click was much faster than that of POC-click and POC. Full degradation of POC-M-click was achieved after 22 weeks (around 5.5 months) of incubation in PBS (pH 7.4), which is much shorter than that of PLLA (~52 weeks, more than 1 year). The fast degradation of POC-M-click can also be confirmed by the *in vivo* study in a rabbit model.

Scaffolds used for tissue regeneration often need to possess good interconnectivity to allow cell penetration and vascular growth in the scaffolds. For our citrate-based polymer family, some traditional pore-forming methods, such as thermally induced phase separation (TIPS), cannot be used due to the low molecular weights of uncrosslinked pre-polymers. A convenient salt-leaching method was often employed in the fabrication of porous citrate-based polymer scaffolds. To improve the interconnectivity of the porous POC-M-click–HA scaffolds, salt particles were first bonded together using PVP, a water- and ethanol-soluble polymer but with poor solubility in 1,4-dioxane, which was used to dissolve POC-M-click pre-polymers (Fig. 1B). The solubility difference of PVP in water and 1,4-dioxane ensured that some aggregates of salt particles bonded with PVP could be kept in the scaffold fabrication process. The morphology of the POC-M-click–HA porous matchstick bone scaffolds was observed under a SEM. As shown in Fig. 3B, there are more interconnected pores and the pore walls are thinner in scaffolds made using PVA for salt bonding than the scaffolds made without using PVP where more dead pores were commonly seen (Fig. 3C). Besides interconnected pores, very thin walls can be found between interconnected or neighbouring pores, which would generate more interconnecting pores along with the fast degradation of the POC-M-click polymer. The improved interconnectivity should benefit cell penetration and proliferation in the scaffolds.[29,30] Favourable attachment and proliferation of BMSCs on the POC-M-click–HA scaffolds was observed after 3 days culture (Fig. 4). At low magnification, a large number of irregularly shaped cells were found attached on the surfaces and pores of the scaffolds. The cells exhibited an irregular and dendritic shape with long spindles while bulging and stretching toward the poles. Some bumps and ridges on the surface of cells were observed, indicating that the cells were firmly adhered to the POC-M-click–HA scaffolds *via* their dendrites (Fig. 4). These results indicate that POC-M-click–HA composites and the degradation products are nontoxic and have good biocompatibility that can physically support the proliferation of BMSCs.

To assess the fusion effect, degradation characteristics, and immunogenicity of the POC-M-click–HA scaffolds *in vivo*, a rabbit intervertebral fusion model was chosen due to its wide adoption in the field, high fusion rate, and favorable repeatability. The animals are relatively inexpensive and easy to manage, and have a short reproduction cycle.[31] Two methods of lumbar fusion are usually adopted: interbody fusion and intertransverse fusion. The intertransverse fusion model has a lower operation risk and a

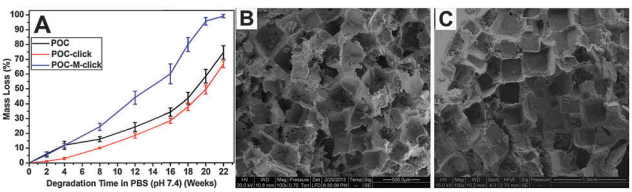

Fig. 3 (A) Degradation profiles of POC-M-click polymer films in PBS (pH 7.4) compared with POC and POC-click polymer films. All polymers were crosslinked at 100 °C for 3 days. Representative SEM images of POC-M-click–HA porous matchstick scaffold fabricated with (B) and without (C) using PVP for salt bonding.

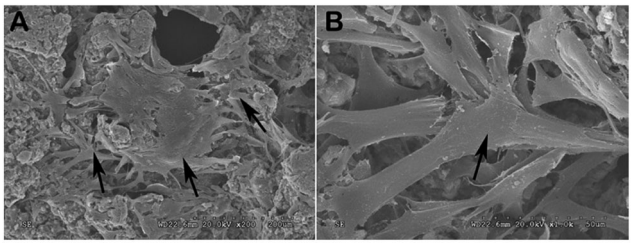

Fig. 4 Scanning electron microscopy (SEM) images of bone marrow-derived mesenchymal stem cells (BMSCs) grown on the POC-M-click–HA scaffolds (3 days) taken at different magnifications: (A) 200× and (B) 1000×.

larger bone graft bed, allowing it to accommodate relatively larger implants. However, the fusion rate for the larger defect in this model is low because of the poor vascular conditions around the transverse processes.[32,33] Compared to the intertransverse fusion model, the interbody fusion model has advantages due to the rich vascular supply at the defect site, which is beneficial for new bone growth. In addition, the results obtained in the interbody fusion model can better represent the clinical situation, as the clinical application of interbody fusion is much more common than intertransverse fusion.[34,35] In the present study, we sought to improve the traditional surgical method by using an anterolateral incision for accessing the target disk and fixation of the vertebral bodies with a specific steel plate (Fig. 2B and C).[36–38] On the other hand, this method simplifies the operative course and prevents translocation of the implant. Moreover, it can provide a relatively stable environment for the fusion, avoiding the interfering effects of rabbits' irregular movements.[36,39]

The spinal fusion performance achieved upon implantation of the three different materials (POC-M-click–HA, PLLA–HA and autologous bone) was evaluated in a rabbit model of intervertebral fusion. The fusion rates observed in each group according to imaging evaluations are listed in Fig. 5C. No migration or breakage of the implant or internal fixation device was observed by X-ray imaging 4 weeks after surgery (Fig. 5A). No obvious new bone formation was observed, but the implants remained in the disc space at this time point.

The fusion rate of the autologous bone group (Group C, 21.3 ± 4.6%) was better than those of both POC-M-click–HA and PLLA–HA groups (Groups A, 11.2 ± 3.7%, and B, 9.3 ± 2.4%), and the difference between groups A and B was not significant ($p > 0.05$, Fig. 5C) at the fourth week. At week 8

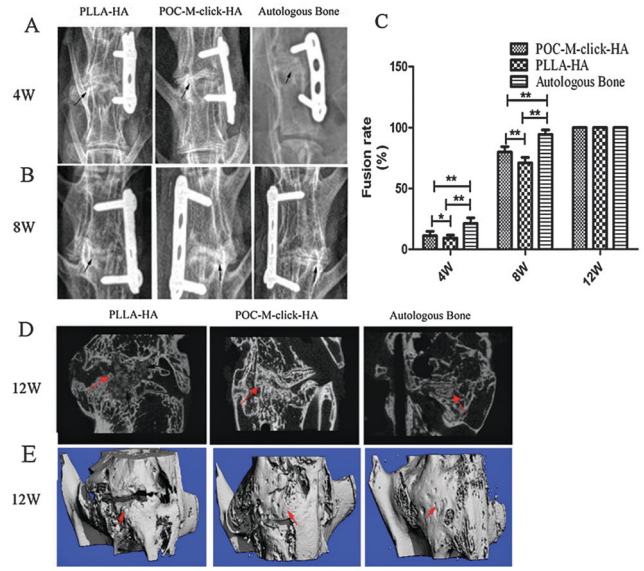

Fig. 5 Radiography observation of spinal fusion. (A and B) Representative X-ray images of specimens at 4 and 8 weeks after surgery. Black arrows indicate the fusion segment. (C) Fusion rate at 4, 8, and 12 weeks (**$p <$ 0.05, *$p >$ 0.05). (D) Representative micro-CT scan along the sagittal plane and (E) three-dimensional reconstruction of a specimen after 12 weeks of surgery with new bone indicated by red arrows.

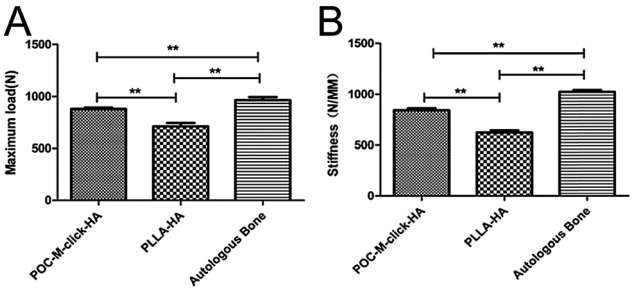

Fig. 6 The maximum bending load (A) and stiffness (B) of the fusion segment 12 weeks after surgery. (**$p < 0.05$).

after operation, the fusion rate of the POC-M-click–HA group (80 ± 4.5%) was significantly higher than that of the PLLA–HA group (71.1 ± 4.4%), although they were both lower than that of the autologous bone group (94.4 ± 3.7%). At 12 weeks after surgery, all specimens in the three groups exhibited an intervertebral fusion rate of 100% according to palpation testing and micro-CT evaluation (Fig. 5D and E).

The results for biomechanical testing of samples harvested 12 weeks after surgery are presented in Fig. 6. The mean maximum load of the POC-M-click–HA group (Group A) was 880.8 ± 14.5 N. Although this value is not as high as that of the autologous bone group, which was 965.2 ± 38.8 N, it is significantly higher than that of the PLLA–HA group (712.0 ± 37.5 N, $p < 0.05$). The fused spinal defect treated with POC-M-click–HA scaffolds also possessed much higher stiffness (843.2 ± 22.4 N mm^{-1}) than that treated with PLLA–HA (622.5 ± 28.4 N mm^{-1}, $p < 0.05$), the stiffness of the fused spine treated with autologous bone grafts was 1024.3 ± 21.5 N mm^{-1}.

Microscopic images of all three groups stained with H&E and Masson's trichrome staining (Fig. 7) showed that new bone formation was visible at the fusion segment at week 12 (Fig. 7b″ and d″), indicating that all three approaches can induce trabecular bone formation. No significant local inflammation response around and in the implanted materials was found at all time-points. After 4 weeks, the POC-M-click–HA implant was surrounded by more new bone than the PLLA–HA implant (Fig. 7b and d), and the POC-M-click–HA material showed partial degradation, leaving behind sporadic cavities (Fig. 7c and d). In contrast, less new bone formation surrounding the PLLA–HA implant and very little material degradation was observed (Fig. 7a and b). After 8 weeks, the POC-M-click–HA composite degraded more, leaving only a small amount of the material inside the new bone (Fig. 7c′ and d′). Similar to the new bone growth observed around the PLLA–HA materials, material degradation was still not obvious (Fig. 7b′). At week 12, in the POC-M-click–HA group, new bone had largely replaced the composite, filled the intervertebral disc space, and connected the upper and lower vertebral bodies as shown by Masson's trichrome staining (Fig. 7d″). The implanted PLLA–HA material also shows new bone formation (Fig. 7b″), but with significantly more residual material surrounding the newly formed bone tissue (Fig. 7a″ and b″).

The results suggest that the POC-M-click–HA material is capable of inducing bone regeneration partly through citrate effects, which is in accordance with our previous studies.[2,19,22]

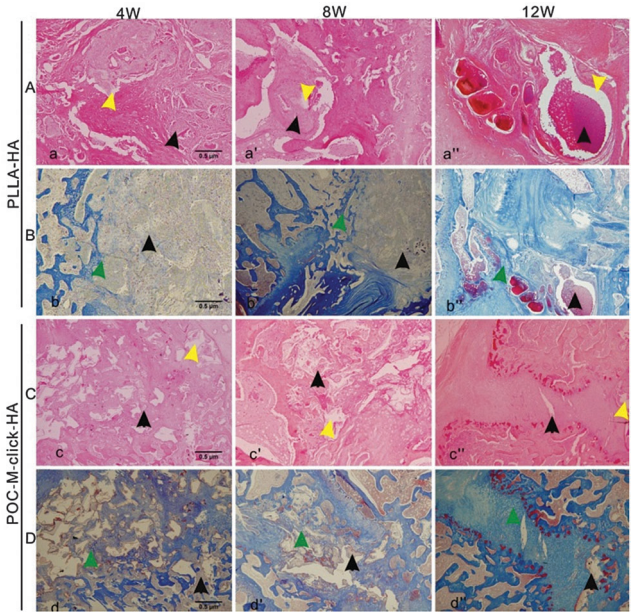

Fig. 7 Photomicrographs of H&E-stained (A and C) and Masson's trichrome-stained (B and D) tissue sections of the explanted PLLA–HA (A and B) and POC-M-click–HA scaffolds (C and D) 4, 8, and 12 weeks after operation. Yellow arrows indicate vacuoles formed upon material degradation and black arrows indicate the residual unabsorbed materials. Green arrows indicate a large amount of new bone formation surrounding the materials.

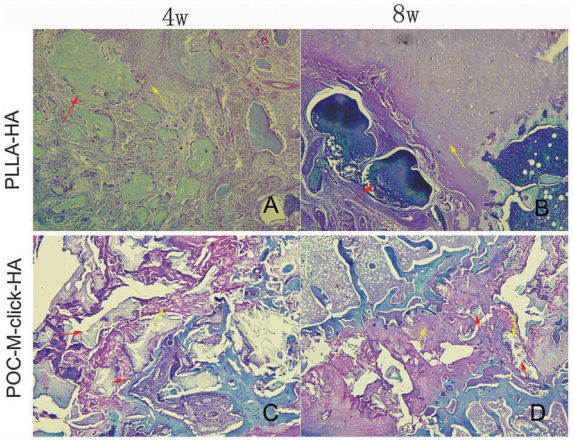

Fig. 8 Photomicrographs of Safranin O/Fast green stained tissue sections of the explanted PLLA-HA (A and B) and POC-M-click–HA scaffolds (C and D) at 4 and 8 weeks after operation. Yellow arrows indicate the cartilage formed surrounding the materials and red arrows indicate the residual unabsorbed materials.

From radiography, μ-CT and histological evaluations, the scaffolds did not release toxic degradation products (Fig. 5–7) during degradation but promoting bone regeneration.

Excitingly, the characteristics of the fusion induced by POC-M-click–HA were much closer to those of autologous bone and significantly better than those of PLLA–HA (Fig. 6), both are widely clinically applied. The POC-M-click–HA composite appeared to serve as a stable intervertebral implant material and the histological staining results suggest that the spinal fusion is a process of cartilage formation and endochondral ossification in the early stage (Fig. 8), with obvious new bone and bone trabeculae formed by 12 weeks (Fig. 7). It was found that chondrocytes grew in the pores of the materials and osteoblast-like cells distributed around the new bone (Fig. 7 and 8). These characteristics are consistent with the physiological process of lumbar fusion.[40] Previous studies showed that pure HA as a bone filling material offered good biocompatibility, but its application is limited by its fragility, poor plasticity, and slow degradation.[13,19] With respect to material degradation, at all three experimental time points, POC-M-click–HA is obviously advantageous over PLLA–HA. Because POC-M-click–HA degrades within an appropriate time scale (completely degraded in 22 weeks in PBS, Fig. 2A), it can not only induce new bone formation at an early stage, but also provide enough space for the growth of new bone and blood vessels as the material degrades. At week four after surgery, no obvious fusion occurred in either the POC-M-click–HA or PLLA–HA group (Fig. 5C, $p > 0.05$). The intervertebral disc spaces were filled primarily with the materials. Newly formed cartilage, confirmed by the baby blue area in the Masson's trichrome staining, was observed surrounding the materials. From H&E staining, it can be seen that POC-M-click–HA partially degraded, with vacuoles within the scaffold area, which is contrary to the PLLA–HA materials that showed no obvious degradation (Fig. 7a and c). At week 8, the fusion rate for the POC-M-click–HA group was significantly higher than that for the PLLA–HA group (Fig. 5C), and these results suggest that POC-M-click–HA induced faster new bone growth. In the meantime, the degradation of POC-M-click–HA at an early stage also contributed to the bone growth. At week 12 after surgery, the new bone had almost completely replaced the POC-M-click–HA scaffold (Fig. 7d″). Although it is shown from Fig. 2A that only around 45 wt% of POC-M-click film degraded after 12 weeks of incubation in PBS, more degradation and absorption of the POC-M-click–HA scaffolds may be expected *in vivo* due to the porous structure and enzymatic environments *in vivo* which may speed up the degradation process. As expected, the released HA particles could be incorporated and remodeled in bone regeneration, which was also confirmed by our previous study.[19] Finally, the biomechanical testing results (Fig. 6) show that in terms of both maximum load and stiffness, the POC-M-click–HA scaffold group is much stronger than the PLLA–HA group and comparable to the autologous bone group showing that POC-M-click–HA facilitated more complete and faster bone formation for spinal fusion compared to PLLA–HA. Excitingly, the performance of the POC-M-click–HA scaffolds resembled the autologous bone grafts in spinal fusion.

3. Conclusions

In conclusion, new mechanically robust, fast degradable citrate-based POC-M-click–HA materials were developed based on the previously developed POC–HA to address the shortage of optimal synthetic bone substitute materials for spinal fusion. Porous POC-M-click–HA composite matchstick scaffolds were fabricated and evaluated in a rabbit lumbar interbody fusion model. Our results showed that the use of the POC-M-click–HA

matchstick scaffolds in spinal fusion elicited minimal inflammatory responses and resulted in faster fusion rates and higher bone biomechanical strengths as compared with PLLA–HA controls. The present work is the first to confirm the promise of citrate-based polymer–HA composites for spinal fusion applications.

4. Materials and methods

4.1 Synthesis of MEDA-modified clickable POC (POC-M-click) pre-polymers

MDEA modified POC-click (POC-M-click) pre-polymers, containing MDEA modified pre-POC-N_3 and pre-POC-Al (pre-POC-M-N_3 and pre-POC-M-Al), were synthesized adapting the procedure described in our previous work (Fig. 1A).[24] The synthesis of pre-POC-M-N_3 is presented here as an example. Briefly, after melting the mixture of citric acid (CA), 1,8-octanediol (OD), and MDEA (molar ratio of CA : OD : MDEA was 1 : 0.8 : 0.1) at 160 °C for 15 min, the reaction temperature was reduced to 120 °C, followed by the addition of diazido-diol monomers (DAzD, 2,2-bis(azidomethyl)propane-1,3-diol, the molar ratio of CA : DAzD was 1 : 0.2). The reaction was continued at 120 °C for ~2 hours. The crude product was purified by precipitating the oligomer–1,4-dioxane solution in water followed by freeze-drying to obtain pre-POC-M-N_3. Pre-POC-M-Al was synthesized by reacting CA, OD, MDEA, and a alkyne diol monomer (AlD, 2,2-bis(hydroxyl-methyl) propionate) instead of DAzD at a molar ratio of 1 : 0.8 : 0.1 : 0.2 using similar protocol described above.

4.2 Degradation study of POC-M-click polymer films

To prepare POC-M-click polymer films for degradation study, equal weights of pre-POC-N_3 and pre-POC-Al were first dissolved in 1,4-dioxane and cast into a Teflon dish to allow solvent evaporation and then crosslinked at 100 °C in an oven for 3 days. Poly(1,8-octanediol citrate) (POC) films and POC-click2 films ("2" represents that the click monomers used, DAzD and AlD, were at 0.2 : 1 [molar ratio] of click monomers to citric acid) were used as controls. These polymers were synthesized as reported in our previous work[24–26] and also crosslinked at 100 °C in an oven for 3 days.

For degradation study, disk-shaped specimens (7 mm in diameter, around 0.15–0.30 mm in thickness) were placed in tubes containing 10 mL of phosphate buffered saline (PBS, pH 7.4) and incubated at 37 °C for pre-set times. After incubation, specimens were washed thoroughly with deionized (DI) water (more than three times) to remove any residual salt before freeze-drying. Mass loss was calculated by eqn (1).

$$\text{Mass loss}\ (\%) = \frac{W_0 - W_t}{W_0} \times 100\% \qquad (1)$$

Here, W_i and W_t are the initial weight and the weight after degradation, respectively. The results are shown in Fig. 2A.

4.3 Fabrication and morphology observation of POC-M-click–HA and PLLA–HA matchstick scaffolds

Porous POC-M-click–HA composite matchstick-shaped scaffolds, with a size of 2 × 2 × 10 mm, HA (from Sigma) content of 65 wt% (weight percentage to the combined weight of HA and polymer), porosity of 65%, and pore size of 250–425 μm, were fabricated using a salt leaching method, as described in Fig. 1B. To improve the interconnectivity, sodium chloride (salt) particles (with a size of 250–425 μm), used as porogen, were first bonded together using polyvinylpyrrolidone (PVP, M_w ~ 10 kDa, from Sigma-Aldrich). PVP (10 v% to the combined amount of salt and PVP) was dissolved in ethanol and the solution was mixed with salt and kept stirring until all the ethanol evaporated. After salt bonding, desired amount of HA (65 wt% of the combined weight of polymer and HA) and POC-M-click pre-polymer solution (equal-weight mixture of pre-POC-M-N_3 and pre-POC-M-Al, 30 wt% in 1,4-dioxane) were mixed together, kept stirring until nearly all the solvent was evaporated. The mixture was kneaded with hands until the composite became dry enough, but still manageable. Matchstick bone scaffolds were made in cuboid Teflon molds with a size of 104 × 2 × 10 mm (width × thickness × length). After drying, the big scaffold was cut into the desired size of 2 × 2 × 10 mm (width × thickness × length) and crosslinked at 100 °C for 3 days to perform a synchronous dual crosslinking process, namely thermal click reaction and esterification. After crosslinking, salt and PVP were leached out by immersing scaffolds in DI water. After salt/PVP leaching, scaffold samples were freeze-dried and sterilized before being used for animal studies. Porous poly(L-lactic acid)–HA (PLLA–HA, PLLA from Polyscitech with a M_w ~ 60 kDa, was used) matchstick scaffolds with the same size (2 × 2 × 10 mm), porosity (65%), HA content (65 wt%) and pore size (250–425 μm) as the POC-M-click–HA scaffolds were also prepared and serve as controls in animal studies.

The morphology of the porous POC-M-click–HA matchstick bone scaffolds was observed using a scanning electron microscope (SEM, FEI Quanta 200 FEG Environmental-SEM, FEI Company, Hillsboro, OR, USA), POC-M-click–HA matchstick bone scaffolds without using PVP for salt bonding were used as controls.

4.4 Experimental animals and grouping

This study was approved by the Ethics Committee of Southern Medical University (Guangzhou, China). Animals were cared for in compliance with the regulations of the Animal Care and Use Committee of Southern Medical University. Specific pathogen-free, healthy New Zealand rabbits were purchased from the Laboratory Animal Center of Southern Medical University. Six rabbits (age, 4–5 weeks) were used only for isolation of bone marrow-derived mesenchymal stem cells (BMSCs). 54 rabbits (average weight, 2–2.5 kg, male or female) were randomly divided into three groups: POC-M-click–HA (Group A, n = 18), PLLA–HA (Group B, n = 18), and autologous bone (Group C, n = 18). All animals were maintained in the Laboratory Animal Centre of Southern Medical University under the same housing conditions.

4.5 BMSC isolation and culture on POC-M-click–HA scaffolds

All operation tools were sterilized using Cobalt-60 for gamma ray sterilization before use. Six rabbits were sacrificed after induction of anesthesia (2% pentobarbital sodium, 20 mg kg^{-1}). Both femurs and tibias of each rabbit were removed and cut at both ends.

Intramedullary contents were extracted using a syringe and dispersed in complete Dulbecco's modified Eagle's medium (DMEM, with 10% fetal bovine serum (FBS)) and centrifuged at 1000 rpm for 5 minutes, followed by the removal of supernatants. The collected bone marrow-derived mesenchymal stem cells (BMSCs) were re-suspended in complete DMEM medium and transferred to Petri dishes. The cell culture media were replaced for the first time after 24 hours and every 2 days thereafter. After reaching 80–90% confluence, the cells were detached with 0.25% trypsin (incubated about 3 minutes) and passaged. The original generation was noted as P0, followed by P1, P2, P3, and so on accordingly.[41] Cells at the third generation were used for culture on the sterilized POC-M-click–HA scaffolds.

BMSCs were first seeded on POC-M-click–HA scaffolds in a 6-well plate with a cell density of 1×10^4 cells per mL (for 1 scaffold with a size of $2 \times 2 \times 10$ mm, using 3 mL), the cell-seeded scaffolds were then moved to a new 6-well plate the next day and cultured for another 7 days in complete DMEM media. The cell culture media were replaced every other day. To observe cell morphology, the cells on the POC-M-click–HA scaffolds were fixed with 4% glutaraldehyde solution for 3 hours, washed with PBS solution, and again fixed in 2% osmic acid, and dried for 1 hour. Then the constructs were dehydrated using a graded ethanol series and then transferred to isoamyl acetate, dried at CO_2 critical point, and observed under a scanning electron microscope (SEM, Dutch PHILIP TEcNAI-10).

4.6 Surgical method

Prior to surgery, rabbits were fasted for 24 hours. The rabbits were sedated with injection of 2% sodium pentobarbital (30 mg kg^{-1}) and prepared for surgery as per standard practice. For autologous bone grafting, an approximately 50 mm^3 bone block was taken from the iliac crest.

For spinal fusion surgery, the rabbits were placed in a lateral position. The L4–L5 transverse processes were exposed and removed through anterolateral surgical intervention to reveal the L4/L5 discs. The L4/L5 discs were then resected. After addressing minor bleeding from the dissected ends, POC-M-click–HA or PLLA–HA matchstick scaffolds were filled in the defects and the L4 and L5 vertebras were then fixed with screws and connected with steel plate (Fig. 2). The wounds were sutured after being washed and tamponed with a gelatin sponge. POC-M-click–HA and PLLA–HA matchstick scaffolds were sterilized by exposing to ethylene oxide overnight before animal surgeries. All animals were given penicillin (50 000 U kg^{-1}) intramuscularly for 3 consecutive days to prevent infection. The rabbits were allowed access to food 24 hours after surgery. Wound healing conditions and hind leg movements were closely observed.

4.7 General observation, X-ray imaging, and micro-computed tomography (micro-CT) evaluation

At 4, 8, and 12 weeks post operation, the rabbits were anaesthetized to obtain lumbar radiographs of the interested area in various views (AP view, lateral view and Flexion-Extension position view) using an X-ray machine (Philips, Netherlands). The position of the tissue construct and spinal fusion for each specimen were evaluated by three advanced radiologists based on the radiographs and stretching palpation tests in a double-blind style based on the Suk's system.[42] Solid union was defined as an obvious intervertebral bone bridge formed when the intervertebral range of motion (ROM) on flexion-extension radiographs was $<4^\circ$. Probable union was confirmed when subtle intervertebral bone bridge was formed, but with $<4^\circ$ intervertebral ROM on flexion-extension radiographs. Fusion nonunion was defined as little or no bone formation between vertebra and the spine, and the motion was beyond 4° on flexion-extension radiographs. At each time point, the number of specimens meeting the standards of solid and probable unions in the three groups was recorded, and the fusion rate for each group at a certain time point was calculated by eqn (2):

$$\text{Fusion rate}\ (\%) = \frac{N_t - N_{non}}{N_t} \times 100 \qquad (2)$$

Here, N_t is the total number of specimens tested and N_{non} is the number of nonunion specimens. For each sample, the fusion rate values obtained by the three experienced radiologists were averaged.

At 12 weeks post operation, all rabbits were sacrificed to obtain the lumbar specimens, which were set for a micro-computer tomography (μ-CT) test and histological examination. μ-CT analysis was conducted using a Micro-CT imaging system (ZKKS-MCT-Sharp-III scanner, Caskaisheng, China) following standard protocols.[19] The scanning system was set to 70 kV, 30 W, and 429 mA. The three-dimensional (3D) images were reconstructed with ZKKS-MicroCT 3.0 software. The spinal fusion performance and bone mass formed between upper and lower endplates were evaluated based on sagittal plane view and 3D reconstructed images.

4.8 Biomechanical testing

The L4–L5 vertebral bodies and intervertebral discs at each time point were removed and stored at −20 °C. Before mechanical testing, the specimens were warmed to room temperature and both ends of the specimen were embedded in poly(methyl methacrylate) (PMMA) to make sure the plane of disc is vertical to the compression direction. The specimens were then fixed on a mechanical tester (Bose Electro Force 3510, USA), and the load was applied at a fixed rate of 0.008 mm s^{-1} for compression tests. The changes of displacement and pressure were recorded. Then values for spinal stiffness and maximum load were calculated.[22]

4.9 Hematoxylin and eosin (H&E) staining and Masson's trichrome staining

Histological examination was performed at pre-determined time points (4, 8, 12 week post-operation) according to previous protocols.[19] After fixation in 4% paraformaldehyde for 1 week, lumbar spine specimens were soaked in ethylenediaminetetraacetic acid (EDTA) decalcified liquid for 4 weeks and then embedded in paraffin for later sections at a thickness of 5–8 μm using a SP2500 microtome (Leica Microsystems, Germany). Sections were then stained by the hematoxylin and eosin (H&E), Masson's trichrome, Safranin O/Fast green staining methods following standard protocols. For both types of stained sections, bone histomorphometric analysis was performed under a semi-automated digitizing image analyzer system consisting of an Olympus BX51 microscope (Center Valley, PA, USA), a computer-coupled QImagingRetigaEXi

camera (Surrey, Canada), and BioQuantOsteo 2009 software (Nashville, TN, USA)

4.10 Statistical analysis

All data are presented as mean ± standard deviation (SD) and differences were tested using the *t*-test. Values of $p < 0.05$ were considered to indicate significant differences between the two groups. Data were analyzed using SPSS 13.0 statistical software (SPSS, Inc., Chicago, IL, USA). The main paragraph text follows directly on here.

Acknowledgements

This work was supported in part by National Institutes of Health (NIH) Awards (EB012575, CA182670, and HL118498), National Science Foundation (NSF) Awards (DMR1313553, CMMI 1266116), and a National Natural Sciences Foundation of China Award (31228007).

Notes and references

1 J. J. Reid, J. S. Johnson and J. C. Wang, *J. Biomech.*, 2011, **44**, 213.
2 D. Sun, Y. Chen, R. T. Tran, S. Xu, D. Xie, C. Jia, Y. Wang, Y. Guo, J. Guo, Z. Zhang, J. Yang, D. Jin and X. Bai, *Sci. Rep.*, 2014, **4**, 6912.
3 Z. Ghogawala, R. G. Whitemore, W. C. Watters 3rd, A. Sharan, P. V. Mummaneni, A. T. Dailey, T. F. Choudhri, J. C. Eck, M. W. Groff, J. C. Wang, D. K. Resnick, S. S. Dhall and M. G. Kaiser, *J. Neurosurg. Spine*, 2014, **21**, 14.
4 B. R. Ransom, E. Neale, M. Henkart, P. N. Bullock and P. G. Nelson, *J. Neurophysiol.*, 1977, **40**, 1132.
5 R. Dimitriou, G. I. Mataliotakis, A. G. Angoules, N. K. Kanakaris and P. V. Giannoudis, *Injury*, 2011, **42**, S3.
6 T. Nakajima, H. Iizuka, S. Tsutsumi, M. Kayakabe and K. Takagishi, *Spine*, 2007, **32**, 2432.
7 J. D. Kretlow and A. G. Mikos, *Tissue Eng.*, 2007, **13**, 927.
8 C. Hou, R. Yang and S. Hou, *J. Hosp. Infect.*, 2005, **59**, 41.
9 M. F. Moreau, Y. Gallois, M. F. Baslé and D. Chappard, *Biomaterials*, 2000, **21**, 369.
10 J. J. Li, D. L. Kaplanb and H. Zreiqat, *J. Mater. Chem. B*, 2014, **2**, 7272.
11 T. Lou, X. Wang, G. Song, Z. Gu and Z. Yang, *Int. J. Biol. Macromol.*, 2014, **69**, 464.
12 W. Yang, S. K. Both, G. L. van Osch, Y. Wang, J. A. Jansen and F. Yang, *Eur. Cells Mater.*, 2014, **27**, 350.
13 M. Stewart, J. F. Welter and V. M. Goldberg, *J. Biomed. Mater. Res., Part A*, 2004, **69**, 1.
14 L. C. Costello, R. B. Franklin, M. A. Reynolds and M. Chellaiah, *Open Bone J.*, 2012, **4**, DOI: 10.2174/1876525401204010027.
15 Y. Y. Hu, A. Rawal and K. Schmidt-Rohr, *Proc. Natl. Acad. Sci. U. S. A.*, 2010, **107**, 22425.
16 Y. Y. Hu, X. Liu, X. Ma, A. Rawal, T. Prozorov, M. Akinc, S. K. Mallapragada and K. Schmidt-Rohr, *Chem. Mater.*, 2011, **23**, 2481.
17 B. Xie and G. H. Nancollas, *Proc. Natl. Acad. Sci. U. S. A.*, 2010, **107**, 22369.
18 R. T. Tran, L. Wang, C. Zhang, M. Huang, W. Tang, C. Zhang, Z. Zhang, D. Jin, B. Banik, J. L. Brown, X. Bai and J. Yang, *J. Biomed. Mater. Res., Part A*, 2014, **102**, 2521.
19 D. Xie, J. Guo, M. R. Mehdizadeh, R. T. Tran, R. Chen, D. Sun, G. Qian, D. Jin, X. Bai and J. Yang, *J. Mater. Chem. B*, 2015, **3**, 387.
20 H. Qiu, J. Yang, P. Kodali, J. Koh and G. A. Ameer, *Biomaterials*, 2006, **27**, 5845.
21 E. J. Chung, P. Kodali, W. Laskin, J. L. Koh and G. A. Ameer, *J. Mater. Sci.: Mater. Med.*, 2011, **22**, 2131.
22 Y. Guo, R. T. Tran, D. Xie, Y. Wang, D. Y. Nguyen, E. Gerhard, J. Guo, J. Tang, Z. Zhang, X. Bai and J. Yang, *J. Biomed. Mater. Res., Part A*, 2015, **103**, 772.
23 D. Gyawali, P. Nair, H. K. Kim and J. Yang, *Biomater. Sci.*, 2013, **1**, 52.
24 J. Guo, Z. Xie, R. T. Tran, D. Xie, D. Jin, X. Bai and J. Yang, *Adv. Mater.*, 2014, **26**, 1906.
25 J. Yang, A. R. Webb, S. J. Pickerill, G. Hageman and G. A. Ameer, *Biomaterials*, 2006, **27**, 1889.
26 J. Yang, A. R. Webb and G. A. Ameer, *Adv. Mater.*, 2004, **16**, 511.
27 L. C. Costello, M. Chellaiah, J. Zou, R. B. Franklin and M. A. Reynolds, *J. Regener. Med. Tissue Eng.*, 2014, **3**, 4, DOI: 10.7243/2050-1218-3-4.
28 V. Arias, A. Höglund, K. Odelius and A. C. Albertsson, *Biomacromolecules*, 2014, **15**, 391.
29 X. Miao and D. Sun, *Materials*, 2010, **3**, 26.
30 M. Schumacher, U. Deisinger, R. Detsch and G. Ziegler, *J. Mater. Sci.: Mater. Med.*, 2010, **21**, 3119.
31 W. R. Walsh, F. Vizesi, G. B. Cornwall, D. Bell, R. Oliver and Y. Yu, *Eur. Spine J.*, 2009, **18**, 1610.
32 M. Palumbo, M. Valdes, A. Robertson, S. Sheikh and P. Lucas, *Spine J.*, 2004, **4**, 287.
33 M. Valdes, M. Palumbo, A. J. Appel, S. McAllister and M. Ehrlich, *Spine J.*, 2004, **4**, 293.
34 P. Ragni and S. T. Lindlholm, *Clin. Orthop.*, 1991, **272**, 292.
35 N. M. Raizman, J. R. O'Brien, K. L. Poehling-Monaghan and W. D. Yu, *J. Am. Acad. Orthop. Surg.*, 2009, **17**, 494.
36 M. Bezer, Y. Yildirim, B. Erol and O. Güven, *Eur. Spine J.*, 2005, **14**, 227.
37 Y. Gu, L. Chen, H. L. Yang, Z. P. Luo and T. S. Tang, *J. Biomed. Mater. Res., Part A*, 2011, **97**, 177.
38 L. Jin, Y. Wan, A. L. Shimer, F. H. Shen and X. J. Li, *Tissue Eng.*, 2012, **3**, 2041731412454420, DOI: 10.1177/2041731412454420.
39 W. E. G. Müller, E. Tolba, H. C. Schröder, M. Neufurth, S. Wang, T. Link, B. Al-Nawasc and X. Wang, *J. Mater. Chem. B*, 2015, **3**, 1722.
40 S. D. Boden, *Tissue Eng.*, 2000, **6**, 383.
41 J. W. Larson 3rd, E. A. Levicoff, L. G. Gilbertson and J. D. Kang, *J. Bone Jt. Surg., Am. Vol.*, 2006, **88**(suppl 2), 83.
42 S. I. Suk, C. K. Lee, W. J. Kim, J. H. Lee, K. J. Cho and H. J. Kim, *Spine*, 1997, **1**, 210.

